# Supporting Information

## Dual signal magnification for ultrasensitive biosensing based on well-regulated SERS of AuNTs@AuHg and DSN-assisted amplification

Mengyang Zhang,[a] Mengfei Yao,[a] Junzhe Gong,[a] Zhaoyin Wang,[a] Wenwen Tu*[a] and Zhihui Dai*[a,b]

a. School of Chemistry and Materials Science, Nanjing Normal University, Nanjing, 210023, P. R. China.

b. School of Chemistry and Molecular Engineering, Nanjing Tech. University, Nanjing, 211816, P. R. China

*Tel: +86-25-85891051. E-mail: daizhihuii@njnu.edu.cn (Z. Dai); wwt@njnu.edu.cn (W. Tu)

## Table of contents:

## 1. Experimental procedures

**1.1. Chemical and materials:** Chloroauric acid ($HAuCl_4$) and sodium borohydride ($NaBH_4$) were purchased from Sigma-Aldrich Co., Ltd. (Shanghai, China). Hexadecyl trimethyl ammonium chloride (CTAC), crystal violet (CV), L-Ascorbic acid (AA), and magnesium chloride hexahydrate ($MgCl_2 \cdot 6H_2O$) were bought from Sinopharm Chemical Reagent Co. Ltd. (Shanghai, China). Tris(hydroxymethyl)aminomethane (Tris) was provided by Alfa Aesar (Beijing, China). Sodium iodide dihydrate ($NaI \cdot 2H_2O$) was purchased from Xilong Scientific Corporation (Guangdong, China). Cy5-labeled oligonucleotides (5'-Cy5-CAACATCAGTCTGATAAGCTA) were acquired and purified with high-performance liquid chromatography (HPLC) by Shanghai Sangon Biological Engineering Technology and Services Co., Ltd. (Shanghai, China). Ethylene diamine tetraacetic acid (EDTA), diethylpyrocarbonate (DEPC)-treated water (RNase-free), and duplex-specific nuclease (DSN) were purchased from Evrogen Joint Stock Company (Moscow, Russia). MiRNA-21 (UAGCUUAUCAGACUGAUGUUGA), 1-mis-miRNA-21 (UAGCUUAUCACACUGAUGUUGA) and 3-mis-miRNA-21 (UCGCUUAUCACACUGAUGUCGA) were synthesized by Genepharma company (Shanghai, China). Tris-HCl buffered saline (50 mM, pH 8.0) contained 5 mM $MgCl_2$. The above analytical reagents were used without further purification. MiRNAs were diluted with DEPC-treated water, other reagents were prepared with ultrapure water (18.2 MΩ cm) from a Milli-Q purification system (Merck, France).

**1.2. Apparatus:** The transmission electron microscopy (TEM) images, high-resolution transmission electron microscopy (HRTEM) images, and element distribution images were obtained with a JEOL-2100F (JEOL, Japan) at at an accelerating voltage of 200 kV. Energy dispersive X-ray spectroscopy (EDS) were characterized using a JEM-200CX instrument (JEOL, Japan) using an accelerating voltage of 200 kV. All of the electron microscope samples were preparated on the copper mesh. The X-ray crystal powder diffraction (XRD) pattern was

obtained using a D/Max 2500 VL/PC diffractometer (Rigaku, Japan) with a scanning range of 30°-80°. The dynamic light scattering (DLS) was measured by using the Malvern Zetasizer Ultra and the zeta potential measurements were gained on a Nano-z analyzer (Malvern, UK).The ultraviolet-visible (UV-Vis) absorption spectra were recorded on a Cary 60 spectrometer (Agilent, USA). The fluorescence measurements were carried out on a Fluoromax-4 spectrometer (Horiba, France). The emission spectra were recorded from 653 nm to 800 nm with 643 nm excitation and the slit width of the spectrofluorimeter was 5 nm. Fourier transform infrared (FTIR) spectra were obtained with Tensor 27 (Bruker, Germany). Raman spectra were recorded by a LabRAM HR 800 micro spectrometer (Horiba Jobin Yvon) with 633 nm and 785 nm laser lines, 50×objective, and 0.55 numerical-aperture. The laser power was 100% for excitation. The acquisition time of each SERS spectrum was 30 s and the scanning range was from 300 to 1300 $cm^{-1}$. The confocal hole was set to 200 μm. All Raman tests were completed at a constant temperature of 20 ℃.

**1.3. Synthesis of gold nanotriangles:** Gold nanotriangles (AuNTs) were synthesized according to the modified method[S1] which can be roughly divided into three steps: seeds nucleate gradually, nanoparticles grow steady and AuNTs were purified, respectively.

**1.4. Dialysis process and SERS performance of AuNTs:** AuNTs were further purified using the dialysis bags (5 kDa) in a beaker of ultrapure water, which was kept at room temperature for changing the ultrapure water at intervals of 2, 4, 6, 8, 10, and 12 hours. After dialysis, AuNTs solution were incubated with CV, and then SERS measurements of AuNTs were performed with a 633 nm HeNe excitation laser.

**1.5. Preparation of AuNTs@AuHg:** 100 μL $Hg^{2+}$ (2.0 μM) was mixed with 100 μL AuNTs aqueous solution, and then incubated with 100 μL of freshly prepared $NaBH_4$ solution (500 μM). The reacted solution was kept at room temperature for 1 h in the dark.[S2] After that, it was centrifuged at 5000 rpm for 5 min to remove excess unreacted reagent. Finally, AuNTs@AuHg solution were obtained by resuspending the precipitation in 180 μL of ultrapure water.

**1.6. Investigation of Raman enhancement effect of $Hg^{2+}$ on AuNTs:** Raman enhancement effect of different $Hg^{2+}$concentrations (0, 1.0, 1.3, 1.5, 1.8, 2.0, 2.2, 2.6, 2.8, 3.0, 5.0, 10.0, 20.0 μM) on AuNTs were explored and the preparation procedure was as same as that of AuNTs@AuHg. Subsequently, 100 μL CV solution (50 μM) was added into the above solution. After the mixture was incubated for 1 h, the solution was centrifuged at 3000 rpm for 5 min once again. The resulting precipitation was resuspended in 100 μL ultrapure water. Afterwards, Raman spectra of $Hg^{2+}$ were recorded under excitation of 633 nm laser and repeated at the same conditions at least 3 times.

**1.7. Evaluation of anti-aggregation of AuNTs@AuHg toward NaCl:** 100 μL $Hg^{2+}$ (2.0 μM) and 100 μL AuNTs solution were incubated with 100 μL $NaBH_4$ (500 μM) at room temperature for 60 min. After centrifuging at 5000 rpm for 5 min, the precipitation was resuspended with 100 μL NaCl at different concentrations (0, 10, 40, 60, 80 mM) for UV-vis measurements.

**1.8. Construction of SERS biosensor and measurement procedures:** 5 μL of probe DNA (pDNA) (5 μM) was mixed with 40 μL AuNTs@AuHg, and incubated for 7 h at 4 ℃. Subsequently, 4 μL of Tris-HCl buffered saline (50 mM, pH 8.0) containing $MgCl_2$ (5 mM), 1 μL of 0.1 U DSN (buffer), 4 μL of DEPC treated water and 6 μL of miRNA-21 with different concentrations (0 fM, 20 fM, 40 fM, 200 fM, 2 pM 12 pM, 40 pM, 120 pM, 200 pM) were added into AuNTs@AuHg/pDNA solution. After AuNTs@AuHg/pDNA/miRNA-21 were put in a metal bath at 37 ℃ for 120 min, 2 μL of 10×EDTA solution was added into the mixture for 20 min to terminate the amplification reaction.[S3-S5] Finally, AuNTs@AuHg/pDNA/miRNA-21 were performed under excitation of 785 nm laser to complete SERS biosensing for miRNA-21. The detection process of the other two miRNAs were the same as that of miRNA-21.

## 2. Results and discussion

### 2.1. Characterization of AuNTs:

As shown in Fig. S1, AuNTs displayed uniform morphology and favorable

monodispersion, which was consistent with the previous work,[S1] indicating the successful preparation of AuNTs. UV-vis spectroscopy was operated to investigate the optical performance of AuNTs, which illustrated the purification level of materials. An obvious shoulder peak around 550 nm in supernatant suggested that impurity particles were removed by flocculation sedimentation.[S1] In addition, an intensive absorption peak appeared around 660 nm, suggesting AuNTs (precipitation) were purified successfully for future use.

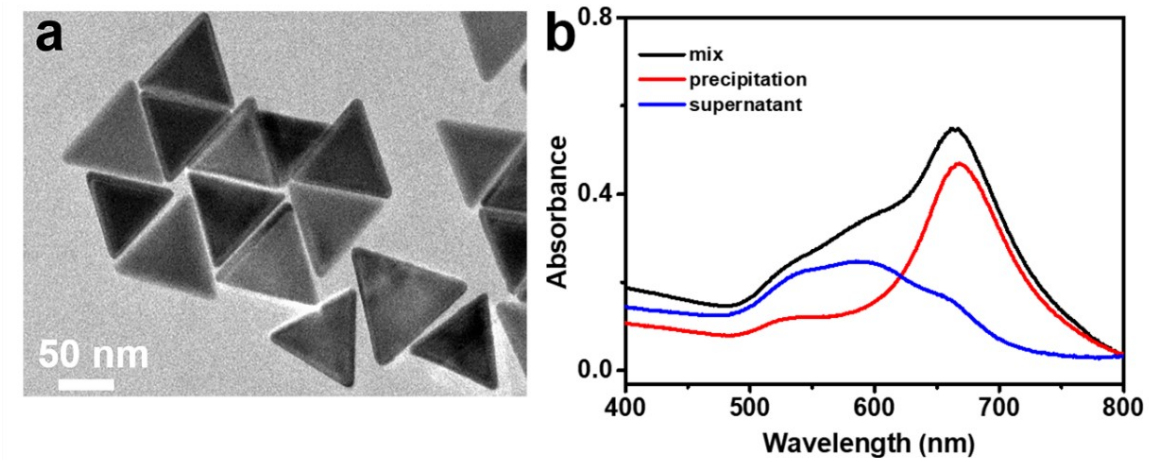


**Fig. S1** (a) TEM micrograph and (b) UV-vis spectra of AuNTs at wavelengths of 400-800 nm before (mix) and after purification (precipitation and supernatant).

**2.2. SERS performance of AuNTs:**

In order to obtain optimal enhancement performance of AuNTs (triangular precipitation), CV was modified with three kinds of solution: mix (red line), precipitation (blue line) and supernatant (green line), respectively and the measurements were carried out with three different lasers. As shown in Fig. S2, Raman signals were obviously enhanced under 532 nm excitation (Fig. S2a), while the results were received under 785 nm excitation with no remarkable enhancement in all three solutions (Fig. S2c). Nevertheless, the occurrence of increased Raman signals under 532 nm excitation displayed hardly selectivity (Fig. S2a). The phenomena indicated that the lasers of both 532 nm and 785 nm did not meet the requirement of tuning SERS properties. However, the precipitation exhibited a selectively increased Raman

signals under the illumination of 633 nm (Fig. S2b), suggesting that 633 nm could be chosen as an optimal wavelength of laser source for obtaining satisfactory enhancement performance of AuNTs.

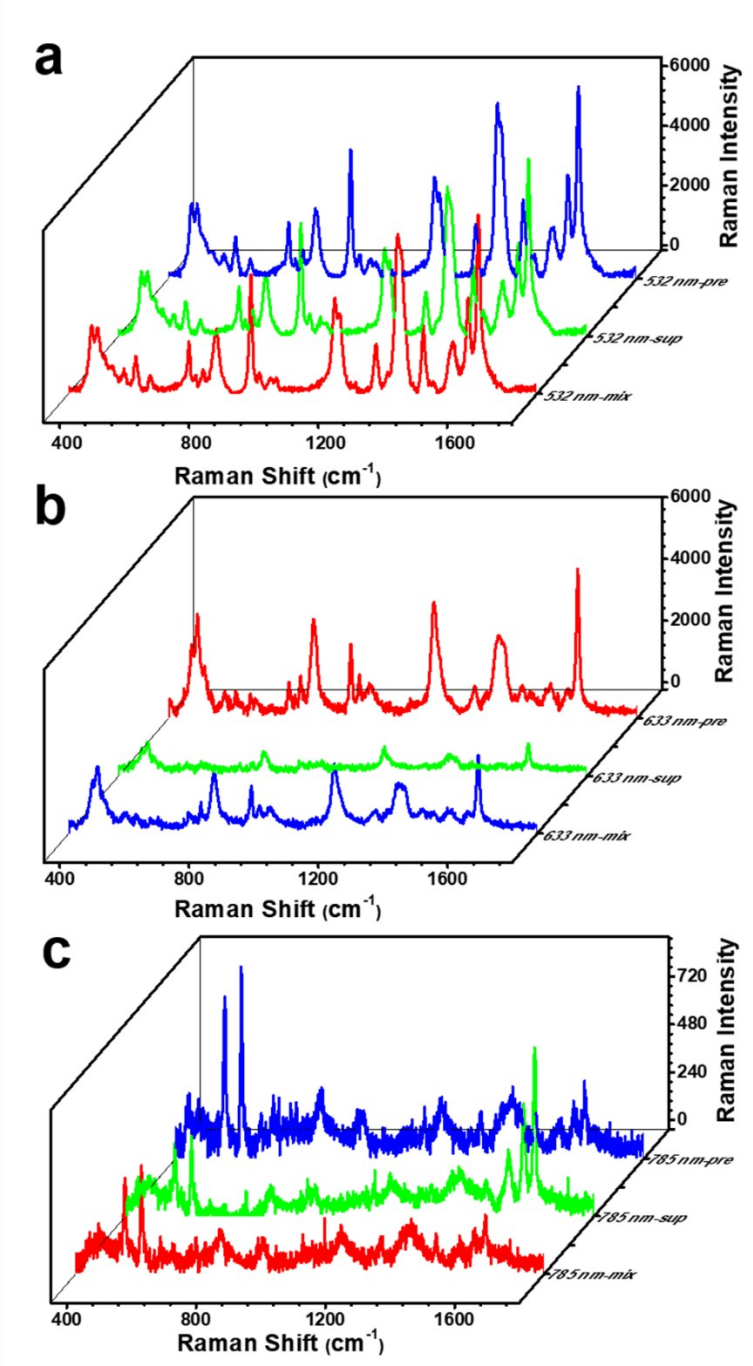


**Fig. S2** SERS spectra of CV-labeled AuNTs before (mix: red line) and after purification (precipitation: blue line and supernatant: green line) at different excitation wavelengths of (a) 532 nm, (b) 633 nm and (c) 785 nm, respectively.

## 2.3. UV-vis absorption spectra of AuNTs@AuHg:

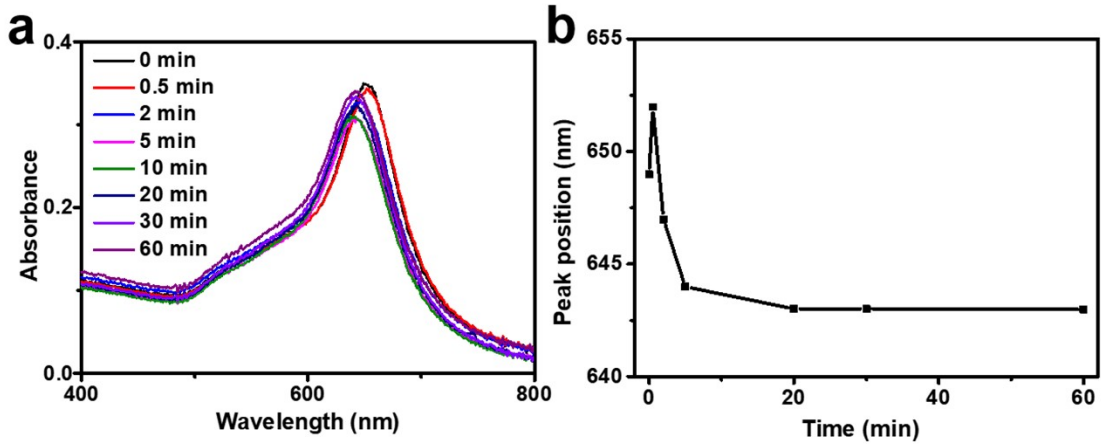


**Fig. S3** (a) UV-vis absorption spectra, and (b) maximum absorption peak position of AuNTs versus different reaction times with $Hg^{2+}$ solution (0.67 μM).

UV-vis absorption spectra were performed to investigate the structure of AuNTs@AuHg (Fig S3). Compared with the inexistence of $Hg^{2+}$ solution (0 min), a bathochromic-shift (2.9 nm) of the maximum absorption peak was observed with the addition of $Hg^{2+}$ solution after 0.5 min, which indicated Hg might be deposited on the surface of AuNTs. Nevertheless, after the inward diffusion of Hg, progressively smaller hypochromatic shift of the maximum absorption peak appeared from 0.5 to 20 min, and then it leveled off over 20 min. The shift of maximum absorption peak position of AuNTs might be inferred the formation of AuNTs@AuHg alloy via in situ reduction of $Hg^{2+}$ on AuNTs.[S6-S8]

## 2.4. Elemental mapping images of AuNTs@AuHg:

STEM and elemental mapping were applied to characterize the element distribution of the AuNTs@AuHg (Fig. S4). The results of STEM and elemental mapping images probably revealed the successful formation of AuNTs@AuHg alloy by quantifying the elemental contribution of Au (Fig. S4b) and Hg (Fig. S4c) related to the total signal, which suggested in situ reduction of $Hg^{2+}$ on AuNTs. In addition, the elemental mapping analyses might confirm that elemental Hg uniformly distributed on AuNTs after amalgamation (AuNTs@AuHg alloy).

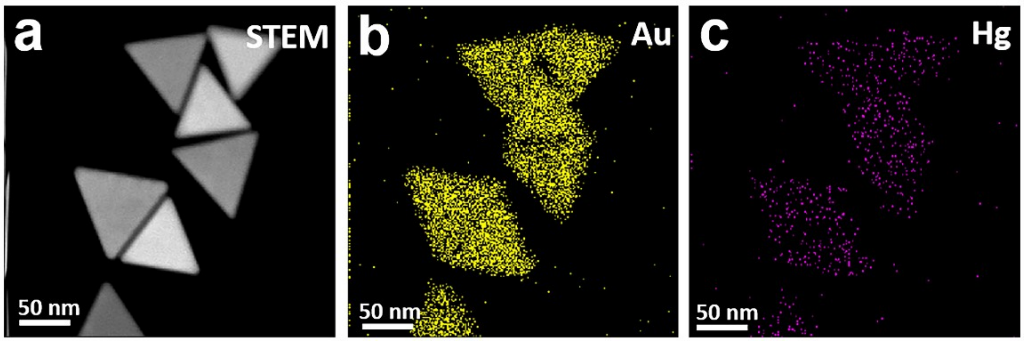


**Fig. S4** (a) STEM image of AuNTs@AuHg, and the elemental mapping images for (b) Au and (c) Hg.

**2.5. EDS spectrum of AuNTs@AuHg:**

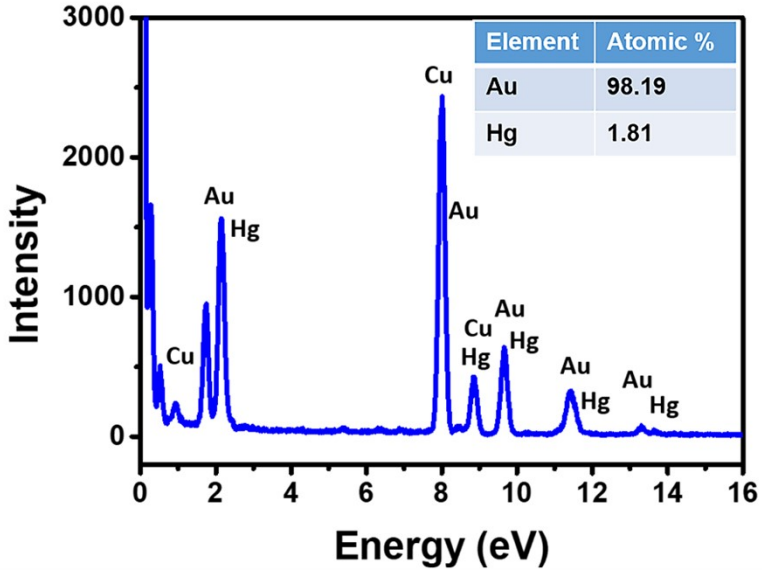


**Fig. S5** Energy dispersive X-ray spectroscopy of AuNTs@AuHg. Inset: atomic percentage of Au and Hg.

EDS spectrum was performed to explore the content of Hg and Au (Fig. S5). Through a semi-quantitative analysis,[S9] the average contents of Au and Hg as the majority elemental composition of AuNTs@AuHg were 98.19 atomic% and 1.81 atomic%, respectively, which might further verify the successful preparation of AuNTs@AuHg alloy.

**2.6. XRD patterns of AuNTs and AuNTs@AuHg：**

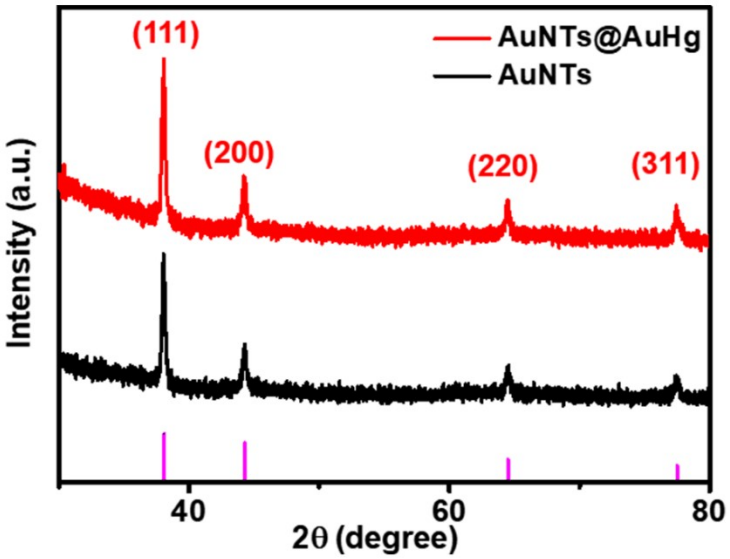


**Fig. S6** X-ray diffraction patterns of AuNTs and AuNTs@AuHg.

The obtained AuNTs and AuNTs@AuHg were further analyzed by XRD technology (Fig. S6). Four characteristic peaks were observed at 38.2°, 44.5°, 64.7°, and 77.7°, which correspond to the (111), (200), (220) and (311) planes of AuNTs.[S10] The diffraction peak of the sample was in accord with the standard card (JCPDS 4-0784), suggesting a face-centered cube arrangement of AuNTs. Moreover, after in situ reduction of $Hg^{2+}$ on AuNTs, the characteristic peaks changed slightly which might be owing to lesser content of Hg on AuNTs@AuHg.

**2.7. TEM and dynamic light scattering characterization of AuNTs@AuHg：**

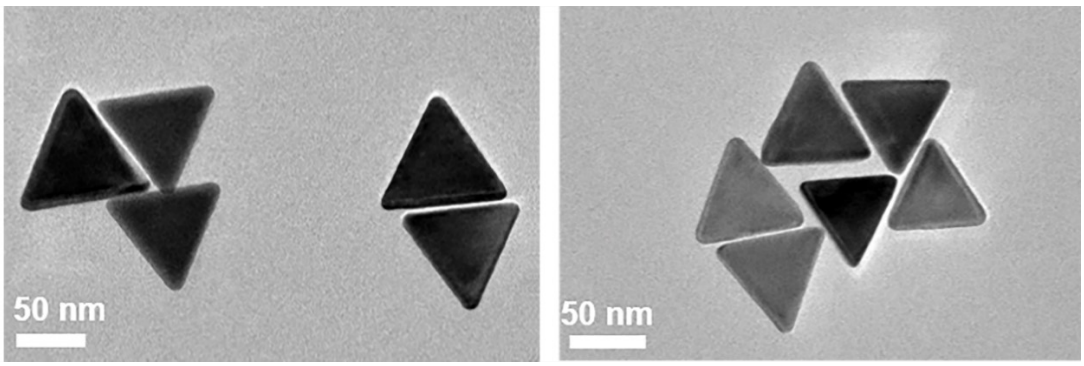

**Fig. S7** TEM images of freshly prepared AuNTs@AuHg (left) and after three days (right), respectively.

TEM (Fig. S7) and dynamic light scattering (Fig. S8) occurring three days apart were applied to attest the long-term stability. Compared with the freshly prepared AuNTs@AuHg, the triangles morphology and size of AuNTs@AuHg hardly altered under $Hg^{2+}$ concentration of 0.67 μM after three days (Fig. S7), indicating a favorable stability. In addition, dynamic light scattering exhibited bimodal distribution bands that had a small band around 10 nm and a much larger band near 100 nm, respectively (Fig. S8). The band of 10 nm might correspond to gold seeds that could not fully grow and another band of 100 nm was ascribed to be AuNTs@AuHg.[S11,S12] After three days, bimodal distribution bands showed a slight shift which meant no aggregation of AuNTs@AuHg, further verifying a satisfactory long-term stability of AuNTs@AuHg.

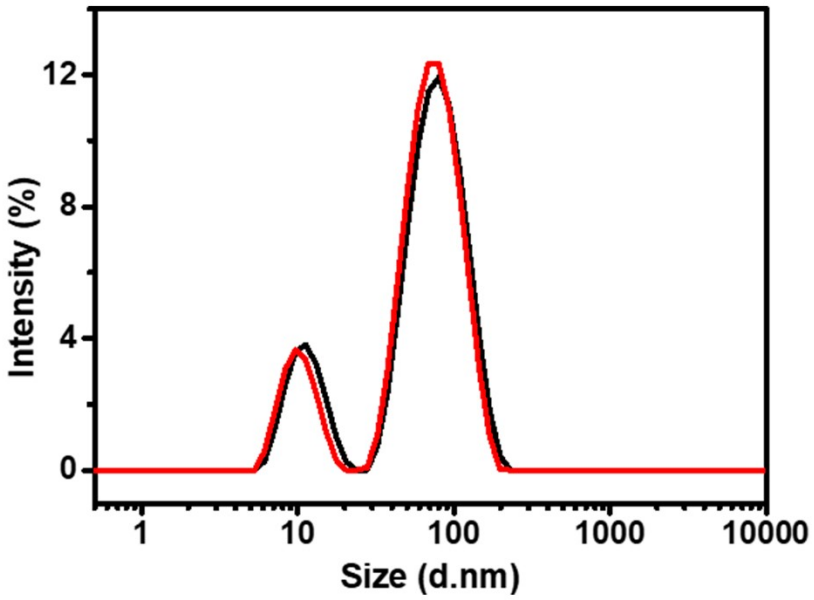


**Fig. S8** Dynamic light scattering representing the particle size distribution of AuNTs@AuHg. Freshly prepared (red line) and after 3 days (black line).

**2.8. The effect of dialysis on Raman response:**

Raman performances of AuNTs before and after dialysis were explored, and the results were displayed in Fig. S9. By taking advantage of a membrane with a molecular weight cut-off (MWCO) of 5 kDa for dialysis of AuNTs substrate, Raman intensity dramatically improved, which confirmed the surfactant on the surface of AuNTs could weaken the SERS response. Therefore, the surfactant should be removed after the preparation of AuNTs as a SERS substrate.

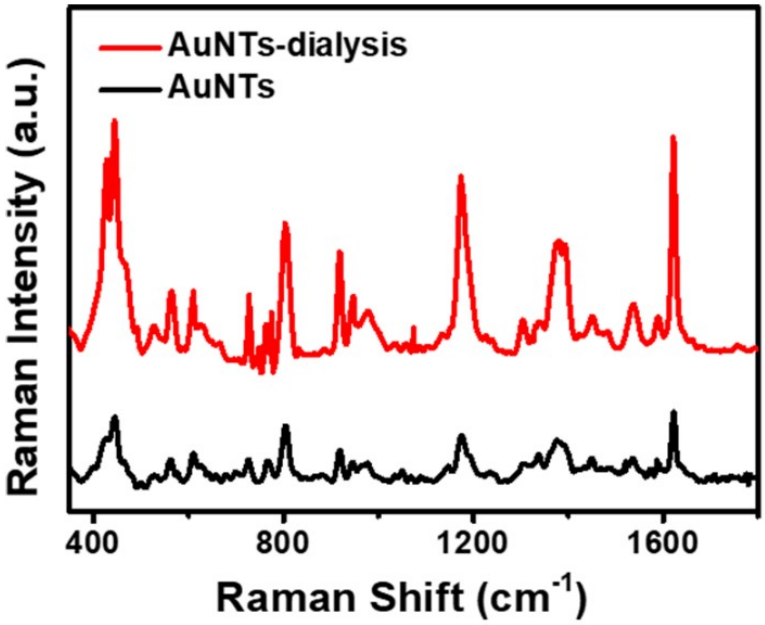


**Fig. S9** SERS responses of CV before (black line) and after (red line) dialysis of AuNTs substrate.

**2.9. Investigation of anti-aggregation and comparison of zeta potential:**

By comparing the shape and intensity of the absorbance spectra, the aggregation of the AuNTs after dialysis (Fig. S10a) and before (Fig. S10b) was investigated in the presence of various NaCl concentrations. Before dialysis, the whole absorption band broadened significantly along with a decrease in overall intensity (Fig. S10b), which suggested that AuNTs might be completely aggregated at the salt concentration of 80 mM. Furthermore, after dialysis of AuNTs, the maximal absorption peak almost disappeared at the salt concentration of 60 mM

(Fig. S10a), indicating that the surfactants of the AuNT surface could act as stabilizing agents for preventing aggregation. While AuHg covered on AuNTs for the substitution of the surfactant, the whole absorption band of AuNTs@AuHg altered slightly with progressively increasing concentrations of NaCl (Fig. S10c), displaying remarkable salt aggregation resistance. Upon addition of $Hg^{2+}$ (0.67 μM), the zeta potential (29.4 mV) of AuNTs@AuHg displayed more positive than that (21.4 mV) of AuNTs (without $Hg^{2+}$) (Fig. S10d), which meant that the electrostatic repulsion on the surface of AuNTs@AuHg was greater than that of the surfactants on AuNTs surface, leading to much improvement of against agglomeration and sedimentation caused by NaCl.

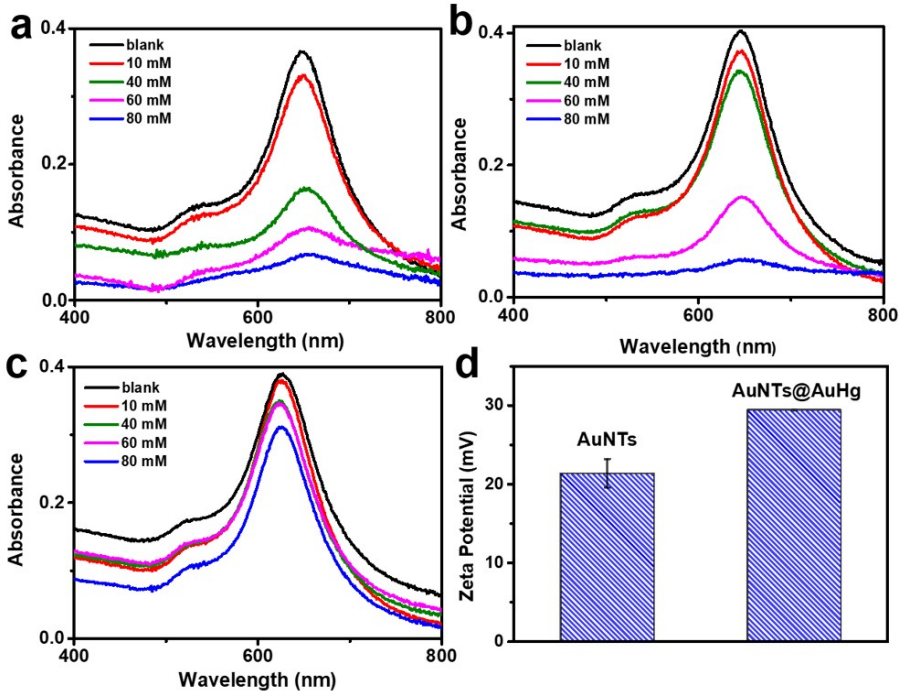


**Fig. S10** UV-vis spectra of AuNTs (after (a) and before (b) dialysis) and AuNTs@AuHg (c) in NaCl solution of different concentrations and (d) zeta potential of AuNTs before dialysis and AuNTs@AuHg (0.67 μM $Hg^{2+}$).

**2.10. SERS responses of the biosensing platform:**

In the absence of DSN, while promoting the concentration of miRNA-21 to 120 pM, no conspicuous difference of SERS response could be observed, compared with that of without miRNA-21 (Fig. S11). This result verified that miRNA-21 could not directly affect the SERS intensity even if its concentration was over 100 pM.

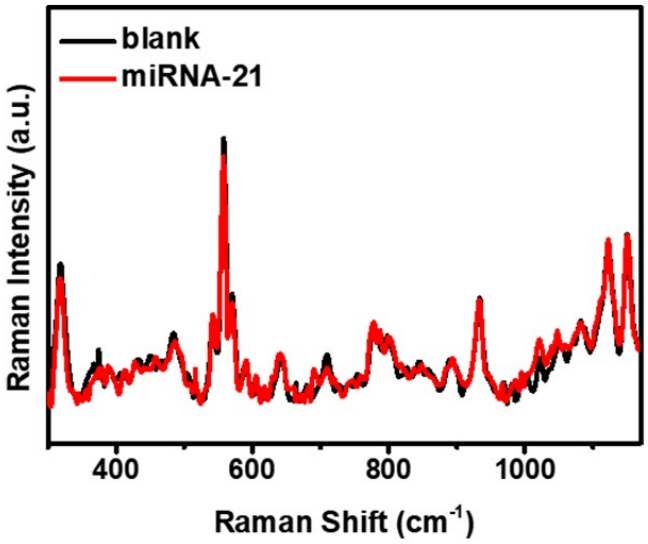


**Fig. S11** SERS responses of the biosensing platform before (black line) and after (red line) incubating with miRNA-21 (120 pM) in the absence of DSN.

### 2.11. SERS biosensing of miRNA:

**Table S1** The performance comparison of the proposed strategy with other methods.

| Analytical method | Detection limit | Detection range | Reference |
|---|---|---|---|
| Fluorescence | 500 fM | 500 fM - 10 pM | S13 |
| Fluorescence | 55 fM | 1 pM - 10 nM | S14 |
| Fluorescence | 8.2 pM | 10 pM - 1000 pM | S15 |
| Electrochemical | 7.78 fM | 100 fM - 100 pM | S16 |
| Electrochemical | 3.5 fM | 10 fM - 100 pM | S17 |
| ECL | 5.7 fM | 0.5 fM - 10 pM | S18 |

| | | | |
|---|---|---|---|
| ECL | 33 fM | 0.1 pM - 100 pM | S19 |
| SERS | 120 fM | 1 pM - 1 nM | S20 |
| SERS | 0.53 fM | 2 fM - 20 pM | This work |

**3. References**


S1 L. Scarabelli and L. M. Liz-Marzán, *ACS Nano*, 2021, **15**, 18600-18607.

S2 J. Lee, G. W. Kim and J. W. Ha, *Analyst*, 2022, **147**, 1066-1070.

S3 Y.-X. Dong, J.-T. Cao, B. Wang, S.-H. Ma and Y.-M. Liu, *ACS Sustainable Chem. Eng.*, 2017, **5**, 10840-10848.

S4 L. Guo, H. Li, R. Zhao, Y. Tang and B. Li, *Chem. Commun.*, 2021, **57**, 5714-5717.

S5 X.-Y. Du, S.-H. Wu, X.-B. Huang and J.-J. Sun, *ACS Appl. Nano Mater.*, 2021, **4**, 2565-2574.

S6 J. Lee, G. W. Kim and J. W. Ha, *Analyst*, 2022, **147**, 1066-1070.

S7 S. F. L. Mertens, M. Gara, A. S. Sologubenko, J. Mayer, S. Szidat, K. W. Krämer, T. Jacob, D. J. Schiffrin and T. Wandlowski, *Adv. Funct. Mater.*, 2011, **21**, 3259-3267.

S8 C. Schopf, A. Martín, M. Schmidt and D. Iacopino, *J. Mater. Chem. C*, 2015, **3**, 8865-8872.

S9 H. Zhang, Q. Ren, S. Mohd, C. Yang, J. Li, Y. Pei and X. Luo, *Sens. Actuator B-Chem.*, 2021, **346**, 130435.

S10 S. Jayabal, R. Sathiyamurthi and R. Ramaraj, *J. Mater. Chem. A*, 2014, **2**, 8918-8925.

S11 I. Kumar, M. Mondal, V. Meyappan and N. Sakthivel, *Mater. Res. Bull.*, 2019, **117**, 18-27.

S12 F. Liebig, R. M. Sarhan, C. Prietzel, A. F. Thünemann, M. Bargheer and J. Koetz, *Langmuir*, 2018, **34**, 4584-4594.

S13 J.-J. Wang, C. Zheng, Y.-Z. Jiang, Z. Zheng, M. Lin, Y. Lin, Z.-L. Zhang, H. Wang and D.-W. Pang, *Anal. Chem.*, 2020, **92**, 830-837.

S14 Q. Li, S. Zhou, T. Zhang, B. Zheng and H. Tang, *Biosens. Bioelectron.*, 2020, **150**, 111866.

S15 X. Li, F. Yang, C. Gan, R. Yuan and Y. Xiang, *Anal. Chem.*, 2021, **93**, 9912-9919.

S16 L. Zhou, T. Wang, Y. Bai, Y. Li, J. Qiu, W. Yu and S. Zhang, *Biosens. Bioelectron.*, 2020, **150**, 111964.

S17 Z. Chen, Y. Xie, W. Huang, C. Qin, A. Yu and G. Lai, *Nanoscale*, 2019, **11**, 11262-11269.

S18 L. Peng, Y. Yuan, X. Fu, A. Fu, P. Zhang, Y. Chai, X. Gan and R. Yuan, *Anal. Chem.*, 2019, **91**, 3239-3245.

S19 H.-Y. Zhu and S.-N. Ding, *Biosens. Bioelectron.*, 2019, **134**, 109-116.

S20 M.-Q. He, S. Chen, K. Yao, K. Wang, Y.-L. Yu and J.-H. Wang, *Small Methods*, 2019, **3**, 1900017.